 CMC, vol.31, no.1, pp.37-64, 2012

Transient Wave Propagation in a Functionally Graded Slab and Multilayered Medium Subjected to Dynamic Loadings

Chien-Ching Ma[1,2], Yi-Hsien Lin[2] and Shih-Hao Lin[2]

Abstract: In this article, the transient response in a functionally graded material (FGM) slab is analyzed by Laplace transform technique. The numerical Laplace inversion (Durbin's formula) is used to calculate the dynamic behavior of the FGM slab. The slab is subjected an uniform loading at the upper surface, and the lower surface are assumed to be traction-free or fixed conditions. The analytical solutions are presented in the transform domain and the numerical Laplace inversion is performed to obtain the transient response in time domain. To take the accuracy and computational efficiency in consideration, Durbin's method is suitable for calculating the long-time response. In addition, the FGM slab is approximated as a multilayered medium with homogeneous material in each layer, and the transient responses of FGM formulation and multilayered solution are discussed in detail.

Keywords: FGM; Multilayered structure; Durbin; Numerical Laplace inversion; Transient response

1 Introduction

In the recent decade, functionally graded materials (FGMs) have drawn considerable attention in engine combustion chamber or nuclear fusion reaction container to reduce the stress concentration or debonding at the interface. An FGM is a particulate composite with continuously changing its thermal and mechanical properties in order to raise the bonding strength in the discrete composite made from different phases of material constituents. For example, in metal-ceramic composite, ceramics can suffer high-temperature environment, but it mismatches with the metal supplying high-toughness. Therefore, FGM has been widely used in the junction and can significantly eliminate thermal residual stresses caused at the interface.

[1] Corresponding author. Tel.: +886-2-23659996; fax:+ 886-2-23631755. E-mail address: ccma@ntu.edu.tw (C. C. Ma)

[2] Department of Mechanical Engineering, National Taiwan University, Taipei, Taiwan 10617, R.O.C.

Most researchers analyzed the composition of FGM with three types, power-law, polynomial, and exponential functions, which are widely used due to the reason that these functions provide convenient process of theoretical investigation. In the literature for FGM with power-law function, Jabbari et al. (2002) provided an analytical solution for steady-state thermal stresses in a hollow thick cylinder made of power-law FGM. Jin and Paulino (2001) presented asymptotic analysis of a power-law FGM strip containing an edge crack under transient thermal loading condition. The second type of FGM for polynomial function were studied by Chiu and Erdogan (1999), Abu-Alshaikh and Köklüce (2006). Chiu and Erdogan (1999) assumed that the stiffness and density of the FGM slab vary continuously with arbitrary polynomial function, and stress wave with a rectangular pressure pulse in nickel-zirconia, and aluminum-silicon media with either free-free or fixed-free boundary conditions was analyzed in detail. Abu-Alshaikh and Köklüce (2006) employed the method of characteristics to solve multilayered-FGM medium varying with polynomial function, the stress response was obtained and compared with results obtained in the literature (Han & Liu, 2002; Han, Liu, & Lam, 2000; Chiu & Erdogan, 1999; Santare, Thamburaj, & Gazoans, 2003). For the third type of FGM, i.e., exponential functions, it was widely used by many authors. Erdogan and Wu (1995) investigated the thermal stress problem of FGM with an exponential-form for an embedded or a surface crack. Jin and Batra (1996) analyzed thermal stresses and the stress intensity factor in an edge-cracked strip of an FGM subjected to sudden cooling at the crack surface. They assumed that the shear modulus decreased hyperbolically from the surface and the thermal conductivity varied exponentially.

The results of fracture mechanics for FGM materials were presented by Delale and Erdogan (1983), Erdogan and Wu (1996), Cai and Bao (1998), and Jin and Paulino (2001). For static problems, Ma and Lee (2009a, 2009b) and Lee and Ma (2010) derived analytical full-field solutions for two-dimensional problem of bi-materials and layered half-plane for functionally graded magnetoelectroelastic materials. FGMs were widely used in many fields in the last 10 years, especially in the mechanical problem of composites in order to avoid the delamination. Therefore, the dynamic problem for wave propagation plays an important role not only in FGM but also in traditionally multilayered media. For one-dimensional wave propagation problem, plane wave propagation in the direction normal to the layered medium, Sun et al. (1968) presented continuum theory instead of "effective modulus theory" to determine dispersion relation. Black et al. (1960) provided a characteristics method for wave propagation in two-layered medium. Lundergan and Drumheller (1971) numerically simulated the response in a layered material system with varying thickness, and their results were in excellent agreement with experiments. Harmonic waves in composites with isotropic layers were also stud-

ied by Stern et al. (1971), Hegemier and Nayfeh (1973). Transient plane waves propagating in a periodically layered elastic medium were examined by Ting and Mukunoki (1979, 1980), and Tang and Ting (1985). Chen et al. (2004) developed an analytical solution based on Floquet's theory to the problem of plate impact in layered heterogeneous material systems, and the comparison between analytical results and experiment data was presented. Liu et al. (1999) investigated One-dimensional elastic waves in an FGM plate excited by plane pressure wavelet, and the material of the FGM plate was assumed to be varying linearly in the thickness direction. Han and Liu (2002) used Fourier transform technique to derive One-dimensional SH-wave propagation in an FGM plate, in which the material properties were assumed as a quadratic function in the thickness direction.

In this paper, the transient response of FGM with polynomial-form is analyzed by Laplace transform technique, and the analytical solutions in the transform domain are presented base on the result obtained by Chiu and Erdogan (1999). By using numerical Laplace inversion from Durbin's method (1974), an effective numerical approach is developed to construct the result of transient-wave propagation in FGM. The analytical-numerical solution presented in this article is based on the Durbin's method for Laplace inversion which differs from the asymptotic approach of Abel-Tauber theorem used by Chiu and Erdogan (1999). The Laplace inversion method is composed of finite Fourier sine and cosine transforms. It is proved in this study that the Durbin's method is capable to perform the long time calculation for transient response with excellent numerical efficiency and accuracy.

In addition, we also analyze a homogeneously multilayered medium to simulate an FGM slab, and determine the transient response for uniformly dynamic loading. Numerical results show that the dynamic behavior for multilayered medium could catch the trend of the transient response for FGM if the FGM is simulated as multilayered homogeneous materials and the number of the layer is greater than ten. The phenomenon of discontinuous caused by impedance-mismatch for multilayered medium is discussed in detail in this study.

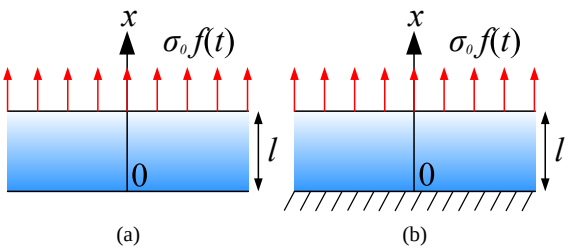

Figure 1: Geometrical configurations and boundary conditions for FGM slabs.

2 Formulation of the Functionally Graded Slab

One-dimensional transient wave propagation in an FGM slab has been derived by Chiu and Erdogan (1999). We briefly follow the derivation made by Chiu and Erdogan (1999) for the solutions in the Laplace transform domain. Consider an initially undisturbed FGM slab as shown in Fig. 1 and the material properties of the FGM slab are assumed to be vary continuously in thickness direction with the following polynomial function

$$E'(x) = E'_0 \left(a\frac{x}{l} + 1\right)^m, \tag{1}$$

$$\rho(x) = \rho_0 \left(a\frac{x}{l} + 1\right)^n, \tag{2}$$

where a, m, n are gradient constants of FGM slab, E', ρ, and l are elastic constant, mass density, and the thickness, respectively. E'_0 and ρ_0 are the elastic constant and density at $x = 0$. For a one-dimensional plane-strain problem with vanishing displacements in the y and z directions, the elastic constant E' can be expressed as the function of Young's modulus and Poisson's ratio as

$$E'(x) = \frac{E(x)(1-\nu(x))}{(1+\nu(x))(1-2\nu(x))}, \tag{3}$$

where E and ν are functions of x. The only non-vanishing displacement u in the x direction and the normal stress σ_{xx} is given by

$$\sigma_{xx} = E'\frac{\partial u}{\partial x}. \tag{4}$$

The wave equation in an inhomogeneous medium can be written as

$$\frac{\partial}{\partial x}\left(E'(x)\frac{\partial u}{\partial x}\right) = \rho(x)\frac{\partial^2 u}{\partial t^2}. \tag{5}$$

The initial conditions for an initially undisturbed FGM slab are presented as

$$u(x,0) = 0, \quad \frac{\partial}{\partial t}u(x,0) = 0. \tag{6}$$

We perform normalized quantities on Eq. (1), (2), (5), and (6)

$$\frac{\partial}{\partial X}\left[(aX+1)^m\frac{\partial U}{\partial X}\right] = (aX+1)^n\frac{\partial^2 U}{\partial T^2}, \tag{7}$$

$$U(X,0)=0, \quad \frac{\partial}{\partial T}U(X,0)=0, \tag{8}$$

where the normalized quantities are

$$X=\frac{x}{l}, \quad U=\frac{u}{l}, \quad T=\frac{c_0 t}{l}, \quad c_0=\sqrt{\frac{E_0'}{\rho_0}}. \tag{9}$$

Eq. (7) is solved by applying Laplace transform over normalized time T with transform parameter p, and the Laplace transform pairs are given by

$$\hat{U}(X,p)=\int_0^{\infty} U(X,T)\,e^{-pT}\,dT, \tag{10a}$$

$$U(X,T)=\frac{1}{2\pi i}\int_{c-i\infty}^{c+i\infty} \hat{U}(X,p)\,e^{pT}\,dp. \tag{10b}$$

The ordinary differential equation for $\hat{U}$ is obtained from Eq. (7) and (8) as follows (Chiu & Erdogan (1999)):

$$\eta^2\frac{d^2\hat{U}}{d\eta^2}+m\eta\frac{d\hat{U}}{d\eta}-\frac{p^2}{a^2}\eta^{n-m+2}\hat{U}=0, \tag{11}$$

where

$$\eta=(aX+1). \tag{12}$$

If $m=n+2$, Eq. (11) will become Euler equation, and the solution of the displacement field in the transform domain can be expressed as

$$\hat{U}(X,p)=C_1(aX+1)^{s_1}+C_2(aX+1)^{s_2}, \tag{13}$$

where

$$s_1,s_2=-\frac{n+1}{2}\pm\sqrt{\left(\frac{n+1}{2}\right)^2+\left(\frac{p}{a}\right)^2}. \tag{14}$$

However, if $m\neq n+2$, the solution of the displacement field is represented in an alternative form as

$$\hat{U}(X,p)=(aX+1)^{\frac{1-m}{2}}\left[C_3\cdot I_{\left|\frac{1-m}{n-m+2}\right|}\left(\left|\frac{2p}{(n-m+2)\,a}\right|(aX+1)^{\frac{n-m+2}{2}}\right)\right.$$
$$\left.+C_4\cdot K_{\left|\frac{1-m}{n-m+2}\right|}\left(\left|\frac{2p}{(n-m+2)\,a}\right|(aX+1)^{\frac{n-m+2}{2}}\right)\right] \tag{15}$$

where I and K are the modified Bessel functions of the first and second kind, respectively. $C_1 \sim C_4$ are undetermined coefficients and can be obtained from the boundary conditions at $x = 0$ and $x = l$. For the case that the bottom surface ($x = 0$) is traction free as shown in Fig. 1(a), the boundary conditions in transform domain can be expressed as follows

$$E' \frac{d}{dX} \hat{U}(0,p) = 0, \text{ at } X = 0, \tag{16}$$

$$E' \frac{d}{dX} \hat{U}(1,p) = \sigma_0 \hat{f}(p), \text{ at } X = 1, \tag{17}$$

where the constant σ_0 is the magnitude of the dynamic loading, and the traction function $\hat{f}$ describes its profile in the transform domain. The coefficients $C_1 \sim C_4$ in Eqs. (13) and (15) can be obtained from Eqs. (16) and (17). The stress fields in the transform domain can be expressed as (Chiu & Erdogan (1999))

$$\frac{\hat{\sigma}_{xx}}{\sigma_0} = \hat{f}(p) \left(\frac{aX+1}{a+1} \right)^{\frac{n+1}{2}} \left\{ \frac{e^{-\delta \cdot [\ln(a+1) - \ln(aX+1)]} - e^{-\delta \cdot [\ln(a+1) + \ln(aX+1)]}}{1 - e^{-2\delta \cdot \ln(a+1)}} \right\} \quad \text{for } m = n+2 \tag{18}$$

$$\frac{\hat{\sigma}_{xx}}{\sigma_0} = \hat{f}(p) \left(\frac{aX+1}{a+1} \right)^{\frac{m+n}{4}} \left[\frac{W_{1x} e^{(z_o - z_x)} - W_{2x} e^{-(z_o - z_x)}}{W_{1l} e^{(z_o - z_l)} - W_{2l} e^{-(z_o - z_l)}} \right] \text{ for } m \neq n+2, \tag{19}$$

where

$$\delta = \sqrt{\left(\frac{n+1}{2} \right)^2 + \left(\frac{p}{a} \right)^2}, \tag{20a}$$

$$z_x = \left| \frac{2p}{(n-m+2)a} \right| (aX+1)^{\frac{n-m+2}{2}}, \tag{20b}$$

$$z_l = \left| \frac{2p}{(n-m+2)a} \right| (a+1)^{\frac{n-m+2}{2}}, \tag{20c}$$

$$z_o = \left| \frac{2p}{(n-m+2)a} \right|, \tag{20d}$$

and the functions W_{1x}, W_{2x}, W_{1l}, and W_{2l} are given as follows

$$
\begin{aligned}
&W_{1x} = \\
&\left[\frac{\sqrt{2\pi z_o}}{e^{z_o}} I_{\nu-1}(z_o) + \frac{\sqrt{2\pi z_o}}{e^{z_o}} I_{\nu+1}(z_o)\right]\left[\sqrt{\frac{2z_x}{\pi}} e^{z_x} K_{\nu-1}(z_x) + \sqrt{\frac{2z_x}{\pi}} e^{z_x} K_{\nu+1}(z_x)\right] \\
&+ \frac{2}{z_o}\left(\frac{m-1}{n-m+2}\right)\left(\frac{\sqrt{2\pi z_o}}{e^{z_o}} I_{\nu-1}(z_o)\right)\cdot\left[\sqrt{\frac{2z_x}{\pi}} e^{z_x} K_{\nu-1}(z_x) + \sqrt{\frac{2z_x}{\pi}} e^{z_x} K_{\nu+1}(z_x)\right] \\
&- \frac{2}{z_o}\left(\frac{m-1}{n-m+2}\right)(aX+1)^{\frac{m-n-2}{2}}\cdot\left(\sqrt{\frac{2z_x}{\pi}} e^{z_x} K_{\nu}(z_x)\right) \\
&\cdot\left[\frac{\sqrt{2\pi z_o}}{e^{z_o}} I_{\nu-1}(z_o) + \frac{\sqrt{2\pi z_o}}{e^{z_o}} I_{\nu+1}(z_o)\right] \\
&- \frac{4}{z_o^2}\left(\frac{m-1}{n-m+2}\right)^2 (aX+1)^{\frac{m-n-2}{2}}\left(\frac{\sqrt{2\pi z_o}}{e^{z_o}} I_{\nu}(z_o)\right)\left(\sqrt{\frac{2z_x}{\pi}} e^{z_x} K_{\nu}(z_x)\right),
\end{aligned}
\tag{21a}
$$

$$
\begin{aligned}
&W_{2x} = \\
&\left[\frac{\sqrt{2\pi z_x}}{e^{z_x}} I_{\nu-1}(z_x) + \frac{\sqrt{2\pi z_x}}{e^{z_x}} I_{\nu+1}(z_x)\right]\left[\sqrt{\frac{2z_o}{\pi}} e^{z_o} K_{\nu-1}(z_o) + \sqrt{\frac{2z_o}{\pi}} e^{z_o} K_{\nu+1}(z_o)\right] \\
&+ \frac{2}{z_o}\left(\frac{m-1}{n-m+2}\right)\left(\frac{\sqrt{2\pi z_x}}{e^{z_x}} I_{\nu-1}(z_x)\right)\cdot\left[\sqrt{\frac{2z_o}{\pi}} e^{z_o} K_{\nu-1}(z_o) + \sqrt{\frac{2z_o}{\pi}} e^{z_o} K_{\nu+1}(z_o)\right] \\
&- \frac{2}{z_o}\left(\frac{m-1}{n-m+2}\right)(aX+1)^{\frac{m-n-2}{2}}\cdot\left(\sqrt{\frac{2z_o}{\pi}} e^{z_o} K_{\nu}(z_o)\right) \\
&\cdot\left[\frac{\sqrt{2\pi z_x}}{e^{z_x}} I_{\nu-1}(z_x) + \frac{\sqrt{2\pi z_x}}{e^{z_x}} I_{\nu+1}(z_x)\right] \\
&- \frac{4}{z_o^2}\left(\frac{m-1}{n-m+2}\right)^2 (aX+1)^{\frac{m-n-2}{2}}\left(\frac{\sqrt{2\pi z_x}}{e^{z_x}} I_{\nu}(z_x)\right)\left(\sqrt{\frac{2z_o}{\pi}} e^{z_o} K_{\nu}(z_o)\right),
\end{aligned}
\tag{21b}
$$

$$
\begin{aligned}
&W_{1l} = \\
&\left[\frac{\sqrt{2\pi z_o}}{e^{z_o}} I_{\nu-1}(z_o) + \frac{\sqrt{2\pi z_o}}{e^{z_o}} I_{\nu+1}(z_o)\right]\left[\sqrt{\frac{2z_l}{\pi}} e^{z_l} K_{\nu-1}(z_l) + \sqrt{\frac{2z_l}{\pi}} e^{z_l} K_{\nu+1}(z_l)\right] \\
&+ \frac{2}{z_o}\left(\frac{m-1}{n-m+2}\right)\left(\frac{\sqrt{2\pi z_o}}{e^{z_o}} I_{\nu-1}(z_o)\right)\cdot\left[\sqrt{\frac{2z_l}{\pi}} e^{z_l} K_{\nu-1}(z_l) + \sqrt{\frac{2z_l}{\pi}} e^{z_l} K_{\nu+1}(z_l)\right] \\
&- \frac{2}{z_o}\left(\frac{m-1}{n-m+2}\right)(a+1)^{\frac{m-n-2}{2}}\cdot\left(\sqrt{\frac{2z_l}{\pi}} e^{z_l} K_{\nu}(z_l)\right) \\
&\cdot\left[\frac{\sqrt{2\pi z_o}}{e^{z_o}} I_{\nu-1}(z_o) + \frac{\sqrt{2\pi z_o}}{e^{z_o}} I_{\nu+1}(z_o)\right] \\
&- \frac{4}{z_o^2}\left(\frac{m-1}{n-m+2}\right)^2 (a+1)^{\frac{m-n-2}{2}}\left(\frac{\sqrt{2\pi z_o}}{e^{z_o}} I_{\nu}(z_o)\right)\left(\sqrt{\frac{2z_l}{\pi}} e^{z_l} K_{\nu}(z_l)\right),
\end{aligned}
\tag{21c}
$$

$$
\begin{aligned}
&W_{2l} = \\
&\left[\frac{\sqrt{2\pi z_l}}{e^{z_l}} I_{\nu-1}(z_l) + \frac{\sqrt{2\pi z_l}}{e^{z_l}} I_{\nu+1}(z_l)\right]\left[\sqrt{\frac{2z_o}{\pi}} e^{z_o} K_{\nu-1}(z_o) + \sqrt{\frac{2z_o}{\pi}} e^{z_o} K_{\nu+1}(z_o)\right] \\
&+ \frac{2}{z_o}\left(\frac{m-1}{n-m+2}\right)\left(\frac{\sqrt{2\pi z_l}}{e^{z_l}} I_{\nu-1}(z_l)\right)\cdot\left[\sqrt{\frac{2z_o}{\pi}} e^{z_o} K_{\nu-1}(z_o) + \sqrt{\frac{2z_o}{\pi}} e^{z_o} K_{\nu+1}(z_o)\right] \\
&- \frac{2}{z_o}\left(\frac{m-1}{n-m+2}\right)(a+1)^{\frac{m-n-2}{2}}\cdot\left(\sqrt{\frac{2z_o}{\pi}} e^{z_o} K_{\nu}(z_o)\right) \\
&\cdot\left[\frac{\sqrt{2\pi z_l}}{e^{z_l}} I_{\nu-1}(z_l) + \frac{\sqrt{2\pi z_l}}{e^{z_l}} I_{\nu+1}(z_l)\right] \\
&- \frac{4}{z_o^2}\left(\frac{m-1}{n-m+2}\right)^2 (a+1)^{\frac{m-n-2}{2}}\left(\frac{\sqrt{2\pi z_l}}{e^{z_l}} I_{\nu}(z_l)\right)\left(\sqrt{\frac{2z_o}{\pi}} e^{z_o} K_{\nu}(z_o)\right).
\end{aligned}
\tag{21d}
$$

For the case that the bottom surface ($x = 0$) is fixed as indicated in Fig. 1(b), we have

$$
\hat{U}(0,p) = 0, \text{ at } X = 0, \tag{22a}
$$

$$E' \frac{d}{dX} \hat{U}(1,p) = \sigma_0 \hat{f}(p), \text{ at } X = 1. \tag{22b}$$

The stress fields in the transform domain for this case can be expressed as (Chiu & Erdogan (1999))

$$\frac{\hat{\sigma}_{xx}}{\sigma_0} = \hat{f}(p) \left(\frac{aX+1}{a+1} \right)^{\frac{n+1}{2}} \left\{ \frac{[-(n+1)+2\delta](aX+1)^{\delta} - [-(n+1)-2\delta](aX+1)^{-\delta}}{[-(n+1)+2\delta](a+1)^{\delta} - [-(n+1)-2\delta](a+1)^{-\delta}} \right\} \quad \text{for } m = n+2, \tag{23}$$

$$\frac{\hat{\sigma}_{xx}}{\sigma_0} = \hat{f}(p) \left(\frac{aX+1}{a+1} \right)^{\frac{m+n}{4}} \left[\frac{W_{3x} e^{(z_o - z_x)} + W_{4x} e^{-(z_o - z_x)}}{W_{3l} e^{(z_o - z_l)} + W_{4l} e^{-(z_o - z_l)}} \right] \text{ for } m \neq n+2, \tag{24}$$

where δ, z_x, z_o, and z_l are defined in Eq. (20). The functions W_{3x}, W_{4x}, W_{3l}, and W_{4l} are given as follows

$$W_{3x} = \left(\frac{\sqrt{2\pi z_o}}{e^{z_o}} I_\nu(z_o) \right) \left[\sqrt{\frac{2z_x}{\pi}} e^{z_x} K_{\nu-1}(z_x) + \sqrt{\frac{2z_x}{\pi}} e^{z_x} K_{\nu+1}(z_x) \right] - \frac{2}{z_o} \left(\frac{m-1}{n-m+2} \right) (aX+1)^{\frac{m-n-2}{2}} \cdot \left(\frac{\sqrt{2\pi z_o}}{e^{z_o}} I_\nu(z_o) \right) \left(\sqrt{\frac{2z_x}{\pi}} e^{z_x} K_\nu(z_x) \right)' \tag{25a}$$

$$W_{4x} = \left(\sqrt{\frac{2z_o}{\pi}} e^{z_o} K_\nu(z_o) \right) \left[\frac{\sqrt{2z_x}}{e^{z_x}} I_{\nu-1}(z_x) + \frac{\sqrt{2\pi z_x}}{e^{z_x}} I_{\nu+1}(z_x) \right] - \frac{2}{z_o} \left(\frac{m-1}{n-m+2} \right) (aX+1)^{\frac{m-n-2}{2}} \cdot \left(\frac{\sqrt{2\pi z_x}}{e^{z_x}} I_\nu(z_o) \right) \left(\sqrt{\frac{2z_o}{\pi}} e^{z_o} K_\nu(z_o) \right)' \tag{25b}$$

$$W_{3l} = \left(\frac{\sqrt{2\pi z_o}}{e^{z_o}} I_\nu(z_o) \right) \left[\sqrt{\frac{2z_l}{\pi}} e^{z_l} K_{\nu-1}(z_l) + \sqrt{\frac{2z_l}{\pi}} e^{z_l} K_{\nu+1}(z_l) \right] - \frac{2}{z_o} \left(\frac{m-1}{n-m+2} \right) (a+1)^{\frac{m-n-2}{2}} \cdot \left(\frac{\sqrt{2\pi z_o}}{e^{z_o}} I_\nu(z_o) \right) \left(\sqrt{\frac{2z_l}{\pi}} e^{z_l} K_\nu(z_l) \right)' \tag{25c}$$

$$W_{4l} = \left(\sqrt{\frac{2z_o}{\pi}}e^{z_o}K_\nu(z_o)\right)\left[\frac{\sqrt{2\pi z_l}}{e^{z_l}}I_{\nu-1}(z_l)+\frac{\sqrt{2\pi z_l}}{e^{z_l}}I_{\nu+1}(z_l)\right]$$
$$-\frac{2}{z_o}\left(\frac{m-1}{n-m+2}\right)(a+1)^{\frac{m-n-2}{2}}\cdot\left(\frac{\sqrt{2\pi z_l}}{e^{z_l}}I_\nu(z_l)\right)\left(\sqrt{\frac{2z_o}{\pi}}e^{z_o}K_\nu(z_o)\right). \tag{25d}$$

We should note that the analytical solutions presented in Eqs. (18), (19), (23), and (24) are all in the Laplace transform domain.

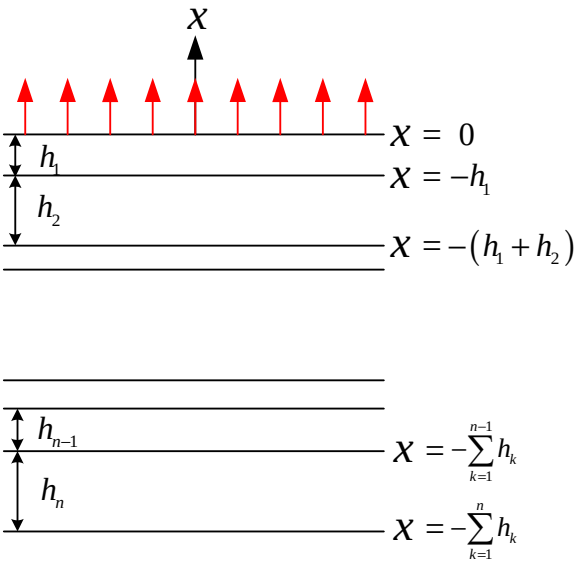

Figure 2: Configuration and coordinate system of an n-layered medium.

3 The FGM Slab is Simulated by Multilayered Homogeneous Medium

In this section, the FGM slab is simulated as a stratified medium consist of n layers as shown in Fig. 2. Each layer is assumed to be elastic, homogeneous, isotropic, and perfectly bonded along the interfaces. The stratified medium is subjected to uniform loadings applied on the top surface at $t = 0$. The quantities related to ith layer are suffixed by a superscript (i), and n stratified layers contains $n+2$ media including upper and lower half-space. In other words, (0) implies the upper half-space and $(n+1)$ implies the lower half-space.

We will consider plane wave propagation in the x direction in which the only non-vanishing component of the displacement is in the x direction, and the 1-D longitu-

dinal wave equation can be expressed as follows:

$$\frac{\partial^2 u}{\partial x^2} = S_L^2 \frac{\partial^2 u}{\partial t^2}, \tag{26}$$

where $u(x,t)$ is the longitudinal displacement and S_L is the slowness of the longitudinal wave given by

$$S_L = \frac{1}{C_L} = \sqrt{\frac{\rho}{(\lambda + 2\mu)}} = \sqrt{\frac{\rho\,(1+\nu)\,(1-2\nu)}{E\,(1-\nu)}},$$

in which C_L, ρ, λ, μ, E and ν are the longitudinal wave velocity, mass density, Lamé constant, shear modulus, Young's modulus and Poisson's ratio, respectively. The boundary conditions on the top and bottom layers of the multilayered medium can be written as

$$\sigma_{xx}^{(1)}(0,t) = \sigma_0 \cdot f(t), \tag{27}$$

$$\sigma_{xx}^{(n)}\left(-\sum_{k=1}^{n} h_k, t\right) = 0, \tag{28}$$

where $f(t)$ is the traction function. The displacement and traction continuity conditions at the interface between two adjacent layers, i.e., ith layer and $(i+1)$th layer, are expressed as follows,

$$u^{(i)}\left(-\sum_{k=1}^{i} h_k, t\right) = u^{(i+1)}\left(-\sum_{k=1}^{i} h_k, t\right) \text{ for } i = 1,2,3,...,n-1, \tag{29}$$

$$\sigma_{xx}^{(i)}\left(-\sum_{k=1}^{i} h_k, t\right) = \sigma_{xx}^{(i+1)}\left(-\sum_{k=1}^{i} h_k, t\right) \text{ for } i = 1,2,3,...,n-1, \tag{30}$$

where the superscripts i in parentheses indicate the field quantities in the ith layer. For instance, $\cdot^{(i)}$ and $\cdot^{(i+1)}$ denote the displacement or stress fields in the ith layer and the (i+1)th layer, respectively. The boundary value problem and continuity conditions described above are solved by applying Laplace transform over time t with transform parameter p. The transform pair of the Laplace transform for a function $u(x,t)$ are given by

$$\hat{u}(x;p) = \int_0^{\infty} u(x,t)\, e^{-pt} dt, \tag{31a}$$

$$u(x,t) = \frac{1}{2\pi i} \int_{c-i\infty}^{c+i\infty} \hat{u}(x;p)\, e^{pt} dp. \tag{31b}$$

Apply the Laplace transform on Eq. (26), the solution of displacement field can be presented as

$$\hat{u}(x;p) = u_-(p)e^{+pS_Lx} + u_+(p)e^{-pS_Lx}, \tag{32}$$

and stress field follows Hooke's law,

$$\hat{\sigma}_{xx}(x;p) = \rho C_L p u_-(p)e^{+pS_Lx} - \rho C_L p u_+(p)e^{-pS_Lx}. \tag{33}$$

Hence, we can rewrite these field quantities in transform domain as the displacement-traction matrix,

$$\begin{bmatrix} \hat{u}(x;p) \\ \hat{\sigma}_{xx}(x;p) \end{bmatrix} = \begin{bmatrix} M_{11}(x;p) & M_{12}(x;p) \\ M_{21}(x;p) & M_{22}(x;p) \end{bmatrix} \begin{bmatrix} u_-(p) \\ u_+(p) \end{bmatrix}, \tag{34}$$

where

$$M_{11}(x;p) = e^{+pS_Lx}, \tag{35}$$

$$M_{12}(x;p) = e^{-pS_Lx}, \tag{36}$$

$$M_{21}(x;p) = \rho C_L p e^{+pS_Lx}, \tag{37}$$

$$M_{22}(x;p) = -\rho C_L p e^{-pS_Lx}, \tag{38}$$

are phase-related receiver elements. In order to avoid complicated mathematical expressions, boundary and interface continuity conditions can be represented as follows:

$$\begin{bmatrix}
0 & 0 & M_{21}^{(1)}(0) & M_{22}^{(1)}(0) & 0 \\
M_{11}^{(1)}(-h_1) & M_{12}^{(1)}(-h_1) & -M_{11}^{(2)}(-h_1) - M_{12}^{(2)}(-h_1) & 0 & \\
M_{21}^{(1)}(-h_1) & M_{22}^{(1)}(-h_1) & -M_{21}^{(2)}(-h_1) - M_{22}^{(2)}(-h_1) & \vdots & \\
\vdots & \vdots & \ddots & \ddots & \ddots \\
\vdots & \vdots & \ddots & \ddots & \ddots \\
0 & \cdots & M_{11}^{(n-1)}\left(-\sum_{k=1}^{n-1} h_k\right) & M_{12}^{(n-1)}\left(-\sum_{k=1}^{n-1} h_k\right) & -M_{11}^{(n)}\left(-\sum_{k=1}^{n-1} h_k\right) \\
0 & \cdots & M_{21}^{(n-1)}\left(-\sum_{k=1}^{n-1} h_k\right) & M_{22}^{(n-1)}\left(-\sum_{k=1}^{n-1} h_k\right) & -M_{21}^{(n)}\left(-\sum_{k=1}^{n-1} h_k\right) \\
0 & \cdots & \cdots & \cdots & \cdots
\end{bmatrix}$$

$$\begin{bmatrix} \cdots & \cdots & 0 \\ \cdots & \cdots & 0 \\ \cdots & \cdots & \vdots \\ & & \vdots \\ & & \vdots \\ -M_{12}^{(n)}\left(-\sum_{k=1}^{n-1} h_k\right) & 0 & 0 \\ -M_{22}^{(n)}\left(-\sum_{k=1}^{n-1} h_k\right) & 0 & 0 \\ 0 & -M_{21}^{(n)}\left(-\sum_{k=1}^{n} h_k\right) & -M_{22}^{(n)}\left(-\sum_{k=1}^{n} h_k\right) \end{bmatrix} \cdot \begin{bmatrix} u_-^{(1)} \\ u_+^{(1)} \\ u_-^{(2)} \\ u_+^{(2)} \\ \vdots \\ \vdots \\ u_-^{(n)} \\ u_+^{(n)} \end{bmatrix} = \begin{bmatrix} \sigma_0 \hat{f}(p) \\ 0 \\ 0 \\ \vdots \\ \vdots \\ \vdots \\ 0 \\ 0 \end{bmatrix} \tag{39}$$

In compact notation, the previous equation is written as

$$\mathbf{M}\mathbf{c} = \hat{\mathbf{t}}, \tag{40}$$

where

$$\mathbf{c} = \begin{pmatrix} u_-^{(1)} & u_+^{(1)} & u_-^{(2)} & u_+^{(2)} & \cdots & u_-^{(n)} & u_+^{(n)} \end{pmatrix}^T, \tag{41}$$

and

$$\hat{\mathbf{t}} = \begin{pmatrix} \sigma_0 \hat{f}(p) & 0 & \cdots & \cdots & 0 \end{pmatrix}^T, \tag{42}$$

and the coefficient matrix $\mathbf{M}$ is a $2n \times 2n$ matrix. Subsequently, Eq. (40) can be solved directly by

$$\mathbf{c} = \mathbf{M}^{-1}\hat{\mathbf{t}}. \tag{43}$$

Once the global field vector $\mathbf{c}$ is obtained, the response functions in each layer can be determined. Furthermore, we can relate the response vector $\mathbf{b}$ to the global field vector $\mathbf{c}$ with a phase-related receiver matrix $\mathbf{R_{cv}}$ by arranging the response functions in each layer into this response vector

$$\mathbf{b}(x;p) = \mathbf{R_{cv}}(x;p) \cdot \mathbf{c}, \tag{44}$$

where the phase-related receiver matrix is given by

$$\mathbf{R_{cv}}(x;p) = \begin{bmatrix} M_{11}^{(1)}(x;p) & M_{12}^{(1)}(x;p) & & & & & & \\ M_{21}^{(1)}(x;p) & M_{22}^{(1)}(x;p) & & & & & & \\ & & M_{11}^{(2)}(x;p) & M_{12}^{(2)}(x;p) & & & & \\ & & M_{21}^{(2)}(x;p) & M_{22}^{(2)}(x;p) & & & & \\ & & & & \ddots & & & \\ & & & & & & M_{11}^{(n)}(x;p) & M_{12}^{(n)}(x;p) \\ & & & & & & M_{21}^{(n)}(x;p) & M_{22}^{(n)}(x;p) \end{bmatrix}. \tag{45}$$

It is noted that **b** is the response vector, which represents the solutions of displacement and normal stress in each layer of the multilayered medium in the transform domain. With the transformed solution at hand, the inverse transform should be performed to obtain the transient solution in time domain. We use numerical inversion from the well-known Durbin's method, which is a combination of finite Fourier sine and cosine transforms, and will be briefly described in the next section.

4 Numerical Laplace Inversion

Transient behavior in time domain could be obtained via the theoretical Laplace transform or the numerical inversion of transformation (Durbin, 1974; Papoulis, 1957; Narayanan & Beskos, 1982). In this paper, the numerical inversion method proposed by Durbin is used. This is a very accurate and efficient method for numerically inverting Laplace-transformed functions and is a combination of both finite Fourier sine and cosine transforms. In Durbin's method, the inverse Laplace transformation of a function $\hat{f}(p)$ is expressed as the following form,

$$\begin{aligned} f(t) &= \frac{1}{2\pi i}\int_{c-i\infty}^{c+i\infty} \hat{f}(p)\, e^{pt} dp \\ &= \frac{2e^{\alpha t}}{T^*}\left\{ -\frac{1}{2} Re\left[\hat{f}(\alpha)\right] + \sum_{k=0}^{\mathrm{N}} Re\left[\hat{f}\left(\alpha + i\frac{2k\pi}{T^*}\right)\right]\cos\left(\frac{2k\pi t}{T^*}\right)\right. \\ &\quad \left. - Im\left[\hat{f}\left(\alpha + i\frac{2k\pi}{T^*}\right)\right]\sin\left(\frac{2k\pi t}{T^*}\right)\right\} \end{aligned} \tag{46}$$

Note that the infinite series involved need only be summed up to a finite number of N terms for convergence. The transform parameter p is composed of real part α and imaginary part $\frac{2k\pi}{T^*}$,

$p = \alpha + ik\frac{2\pi}{T^*} k$=0, 1, 2, 3, ..., N,

in which T^* is the time interval of interest, and equidistant points N is a finite positive integer. It is suggested that one should select $\alpha T^* = 5$ to 10 for good calculation results.

We substitute the solutions in the transform domain for the functionally graded slab (i.e., Eqs. (18), (19), (23), (24)) and the multilayered medium (Eq. (44)) into Durbin's formula, i.e. Eq. (46). The transient response in time domain can be obtained. The computational result and comparison for two formulations will be discussed in detail in the next section. It is noted that the Durbin's method has high accuracy for long time calculation and is capable to calculate transient responses for complicated problems.

5 Numerical Results for the FGM Slab and the Multilayered Medium

In this section, the transient response in a single FGM slab is presented and is verified with the calculation provided by Chiu and Erdogan (1999). The initial pulse with a step function form is applied at the top surface $x = l$ as shown in Fig. 1, and the pressure pulse has the following form

$$\sigma_{xx}(l,t) = \sigma_0 f(t) = -\sigma_0 [H(t) - H(t-t_0)], \tag{47a}$$

or expressed in the transform domain as

$$\hat{f}(p) = -\left[\frac{1}{p} - \frac{e^{-pt_0}}{p}\right], \tag{47b}$$

where $H(t)$ is the heaviside function and the pulse duration is $t_0 = 0.2\mu s$.

We consider an FGM slab with thickness $l = 5mm$. The FGM material constants (Ni/ZrO_2 and Al/SiC) used for numerical calculations are listed in Table 1. Ni/ZrO_2 indicates that an FGM slab consists of nickel and zirconia, and pure nickel is on

Table 1: Material constants of FGMs

	Ni/ZrO_2	ZrO_2/Ni	SiC/Al	Al/SiC
$E_0'\ (GPa)$	286.922	223.728	225.719	105.197
$\rho_0\ (kg/m^3)$	8900	5331	3100	2710
$c_0\ (m/s)$	5678	6478	8533	6230
a	0.14096	−0.12354	−0.53395	1.14568
m	−1.8866	−1.8866	1	1
n	−3.8866	−3.8866	0.17611	0.17611

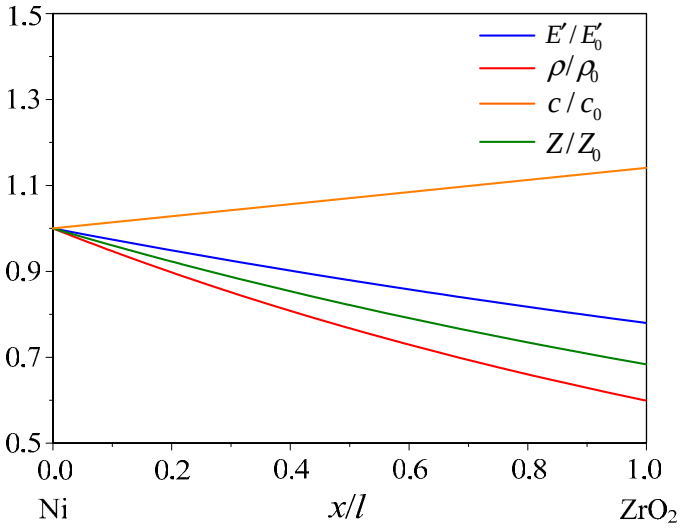

Figure 3: The variation of elastic modulus, density, longitudinal wave velocity, and mechanical impedance in Ni/ZrO_2 FGM.

the bottom surface while the top surface is pure zirconia. For Al/SiC FGM, similarly, Al and SiC are on the bottom surface and top surface, respectively. Fig. 3 shows the material compositions of Ni/ZrO_2 FGM for elastic modulus, density, longitudinal wave velocity, and mechanical impedance along the thickness. Fig. 4 shows these quantities for SiC/Al FGM. It is worthy to note that FGM formulations (Eqs. (18), (19), (23), (24)) and multilayered solution (Eq. (44)) are all presented in the transform domain in previous sections, hence, the numerical Laplace inversion (Durbin's formula) Eq. (46) is used to obtain the transient response in time domain. The numerical results are shown in Figs. 5-15.

5.1 Transient responses of FGM for long-time computation

In Fig. 5, the long-time transient response of Ni/ZrO_2 FGM is evaluated by Durbin's inversion method at the location $x = l/2$ for fixed boundary condition at $x = 0$ (i.e., Fig. 1(b)). Stress response is calculated up to $24\mu s$, and the result is the same as that presented in Chiu and Erdogan (1999) for $12\mu s$. When the pressure pulse travels in FGM and reflects between top and bottom surfaces many times, the step-form pulse is distorted as a needle-like one. The pulse shape is distorted as time increase and the transient response for FGM is completely different from the homogeneous material.

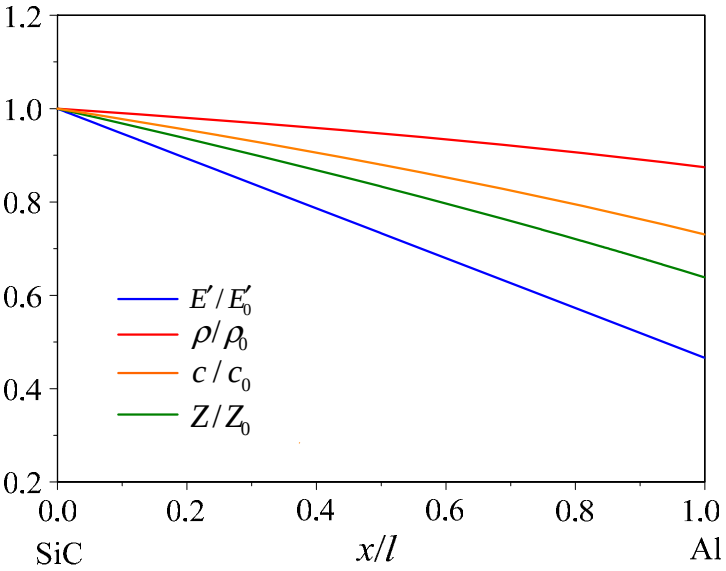

Figure 4: The variation of elastic modulus, density, longitudinal wave velocity, and mechanical impedance in SiC/Al FGM.

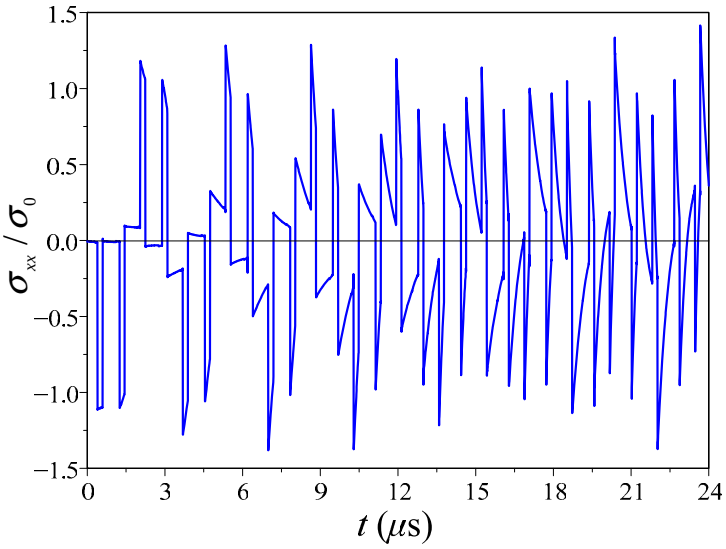

Figure 5: Long-time stress response in a Ni/ZrO_2 FGM slab at $x = l/2$ for fixed boundary condition at $x = 0$.

5.2 An FGM slab is simulated by the multilayered medium

Next, we consider the case that an FGM slab is simulated as a multilayered medium consist of n layers with homogeneous material in each layer. In Eq. (44), we take 10 homogeneous layers with the same thickness to simulate the FGM slab, the response vector $\mathbf{b}$ is a 20×1 vector, the phase-related receiver matrix $\mathbf{R_{cv}}$ is a 20×20 matrix, and the global field vector $\mathbf{c}$ is a 20×1 vector. If we take 20 homogeneous layers with the same thickness to simulate the FGM slab, related matrixes $\mathbf{b}$, $\mathbf{R_{cv}}$, and $\mathbf{c}$ have the size 40×1, 40×40, and 40×1, respectively. Therefore, the matrix-form formulation indicated in Eq. (44) can be worked out and the displacement and stress fields in the transform domain can be determined subsequently. The transient response can be obtained by numerical Laplace inversion (Eq. (46)). For the Durbin's method, computational condition $\alpha T = 7.5$ and the summation terms N=20000 are chosen in Eq. (46) for numerical calculation. The related material constants for 10-layered and 20-layered media are listed in Tables 2-5.

We discuss the situation that $m = n+2$ first. For the case of Ni/ZrO_2 FGM, Fig. 6 presents the transient response at location $x = l/2$ of FGM slab and 10-layered medium for the boundary condition indicated in Fig. 1(a). The source wave arrives at $0.4\mu s$ with magnitude -1.09, and the reflecting wave from the bottom surface of FGM slab arrives at $1.25\mu s$. After that, tensile and compressive stress waves appear alternately and the original step function is distorted as time increases. In the simulation of 10-layered medium, we can see that the influence of stress wave coming from the boundary is larger than that coming from the interface. This phenomenon is due to the fact that the difference of the material constants and the impedance-mismatch of the homogeneous layer is not large. We can see that the transient response for the 10-layered medium displays oscillations around the solution of FGM. However, these oscillations due to impedance-mismatch are growing when more and more waves arrive at the receiver.

For the same case of Ni/ZrO_2 FGM, the transient response at location $x = l/2$ of FGM slab and 10-layered medium for the boundary condition indicated in Fig. 1(b) is expressed in Fig. 7. The transient response for ZrO_2/Ni FGM at location $x = 0$ for the boundary condition indicated in Fig. 1(b) is expressed in Fig. 8. Figures 7 and 8 show the fact that the step pulse in the fixed boundary is distorted more seriously than in the free boundary. The numerical result for 10-layered medium is similar to the FGM formulation except some oscillations appearing in the result of FGM. The transient stress fields for the situation that $m \neq n+2$ (i.e., SiC/Al and Al/SiC) are shown in Figs. 9-11. These figures also indicate that the 10-layered medium can be used to simulate the problem for FGM material.

Next, we compare the results obtained by 10-layered and 20-layered media from

Table 2: The material constants of 10 homogeneous layers to simulate the Ni/ZrO_2 FGM slab

No.	$E(GPa)$	$\rho\ (kg/m^3)$	$C_L\ (m/s)$	Impedance	$h\ (mm)$
1	226.36	5461	6438	35158325	0.5
2	231.76	5733	6358	36451059	0.5
3	237.37	6022	6278	37808617	0.5
4	243.18	6330	6198	39235138	0.5
5	249.22	6658	6118	40735086	0.5
6	255.49	7008	6038	42313275	0.5
7	262.00	7381	5958	43974906	0.5
8	268.77	7779	5878	45725604	0.5
9	275.82	8205	5798	47571454	0.5
10	283.15	8660	5718	49519050	0.5

Table 3: The material constants of 20 homogeneous layers to simulate the Ni/ZrO_2 FGM slab

No.	$E(GPa)$	$\rho\ (kg/m^3)$	$C_L\ (m/s)$	Impedance	$h\ (mm)$
1	225.04	5395	6458	34844813	0.25
2	227.69	5527	6418	35475646	0.25
3	230.39	5663	6378	36121954	0.25
4	233.15	5804	6338	36784215	0.25
5	235.95	5948	6298	37462930	0.25
6	238.80	6097	6258	38158614	0.25
7	241.71	6251	6218	38871805	0.25
8	244.67	6410	6178	39603060	0.25
9	247.69	6574	6138	40352958	0.25
10	250.77	6744	6098	41122101	0.25
11	253.90	6918	6058	41911115	0.25
12	257.09	7099	6018	42720648	0.25
13	260.35	7285	5978	43551376	0.25
14	263.67	7478	5938	44404001	0.25
15	267.06	7677	5898	45279255	0.25
16	270.51	7883	5858	46177897	0.25
17	274.03	8096	5818	47100719	0.25
18	277.62	8316	5778	48048545	0.25
19	281.29	8544	5738	49022231	0.25
20	285.02	8779	5698	50022672	0.25

Table 4: The material constants of 10 homogeneous layers to simulate the SiC/Al FGM slab

No.	$E(GPa)$	$\rho\ (kg/m^3)$	$C_L\ (m/s)$	Impedance	$h\ (mm)$
1	111.22	2737	6375	17446614	0.5
2	123.27	2787	6651	18534735	0.5
3	135.33	2833	6912	19579820	0.5
4	147.38	2876	7159	20587200	0.5
5	159.43	2916	7394	21561164	0.5
6	171.48	2954	7620	22505231	0.5
7	183.54	2989	7836	23422331	0.5
8	195.59	3023	8044	24314933	0.5
9	207.64	3055	8245	25185146	0.5
10	219.69	3085	8438	26034785	0.5

Table 5: The material constants of 20 homogeneous layers to simulate the SiC/Al FGM slab

No.	$E(GPa)$	$\rho\ (kg/m^3)$	$C_L\ (m/s)$	Impedance	$h\ (mm)$
1	108.21	2724	6303	17167107	0.25
2	114.24	2750	6446	17723019	0.25
3	120.26	2775	6584	18266975	0.25
4	126.29	2799	6718	18799811	0.25
5	132.31	2822	6848	19322272	0.25
6	138.34	2844	6975	19835017	0.25
7	144.37	2865	7098	20338640	0.25
8	150.39	2886	7219	20833674	0.25
9	156.42	2906	7337	21320602	0.25
10	162.44	2926	7452	21799860	0.25
11	168.47	2944	7564	22271848	0.25
12	174.50	2963	7675	22736931	0.25
13	180.52	2980	7783	23195442	0.25
14	186.55	2998	7889	23647690	0.25
15	192.58	3015	7993	24093959	0.25
16	198.60	3031	8095	24534510	0.25
17	204.63	3047	8195	24969588	0.25
18	210.65	3063	8294	25399419	0.25
19	216.68	3078	8391	25824214	0.25
20	222.71	3093	8486	26244169	0.25

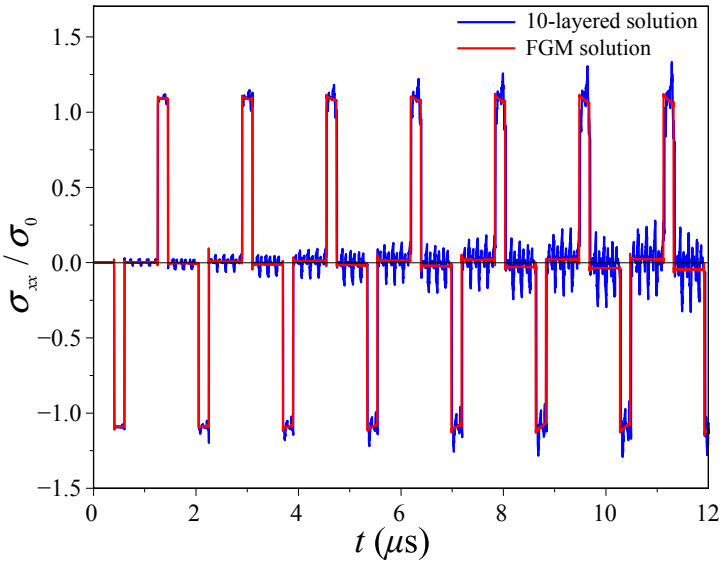

Figure 6: The stress responses in a Ni/ZrO_2 FGM slab and 10-layered medium at $x = l/2$ for free boundary condition at $x = 0$.

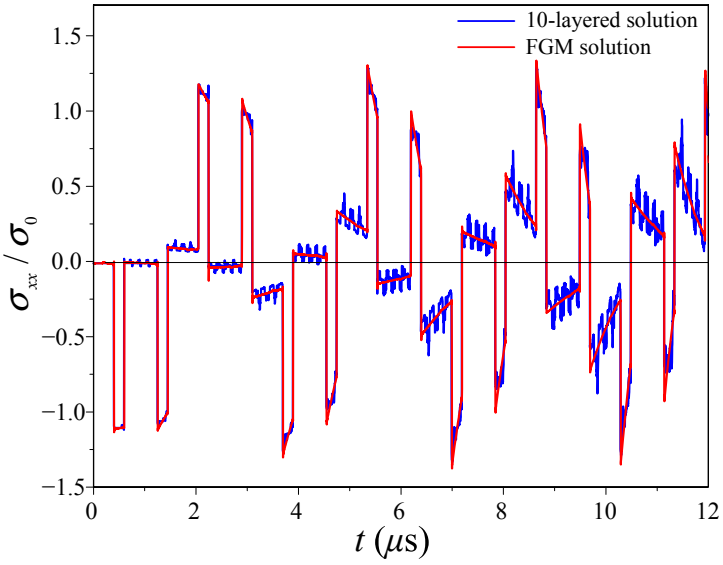

Figure 7: The stress responses in a Ni/ZrO_2 FGM slab and 10-layered medium at $x = l/2$ for fixed boundary condition at $x = 0$.

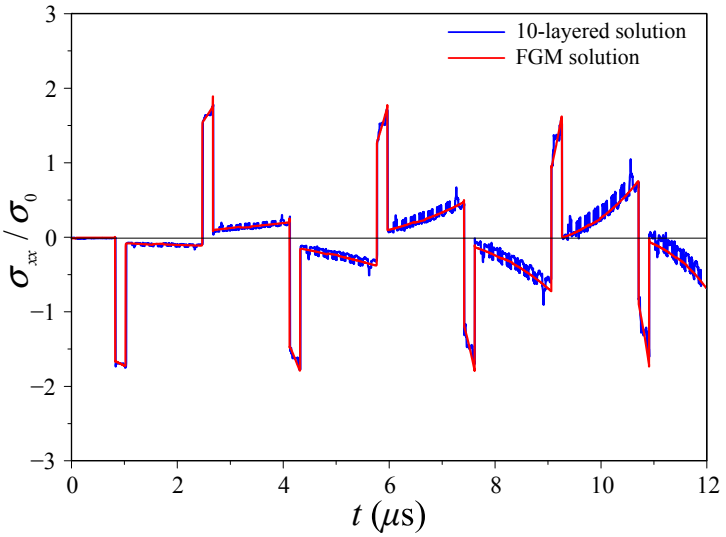

Figure 8: The stress responses in a ZrO_2/Ni FGM slab and 10-layered medium at $x = 0$ for fixed boundary condition at $x = 0$.

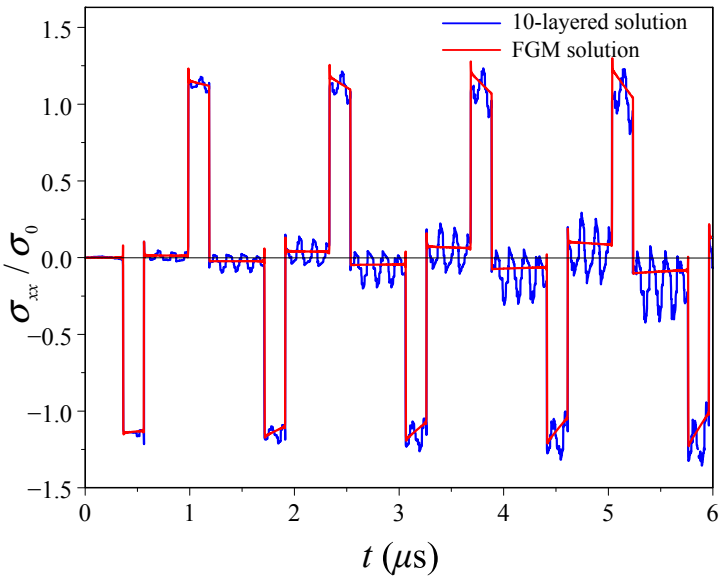

Figure 9: The stress responses in a SiC/Al FGM slab and 10-layered medium at $x = l/2$ for free boundary condition at $x = 0$.

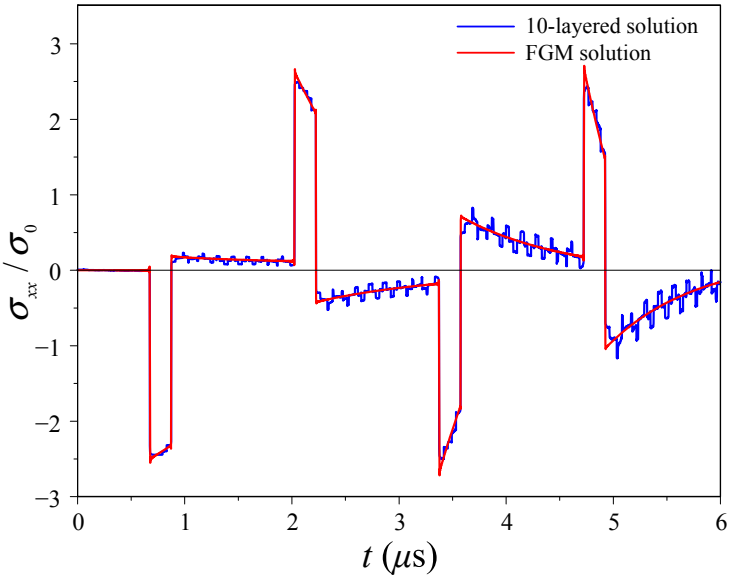

Figure 10: The stress responses in a SiC/Al FGM slab and 10-layered medium at $x = 0$ for fixed boundary condition at $x = 0$.

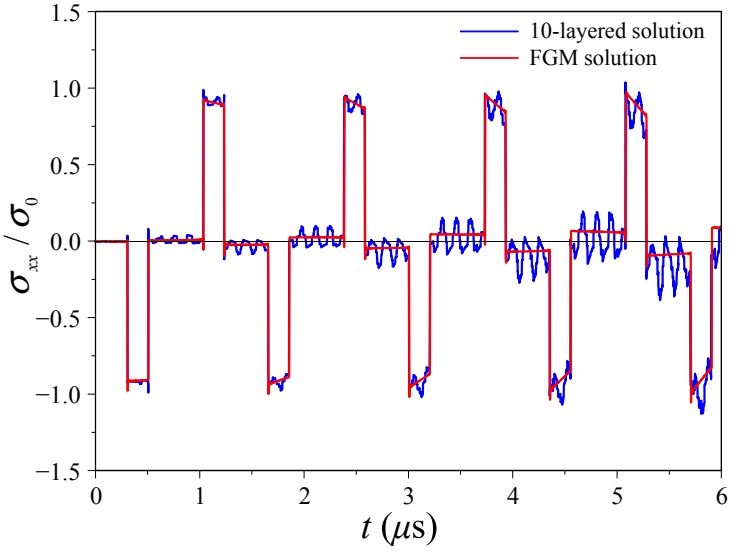

Figure 11: The stress responses in a Al/SiC FGM slab and 10-layered medium at $x = l/2$ for free boundary condition at $x = 0$.

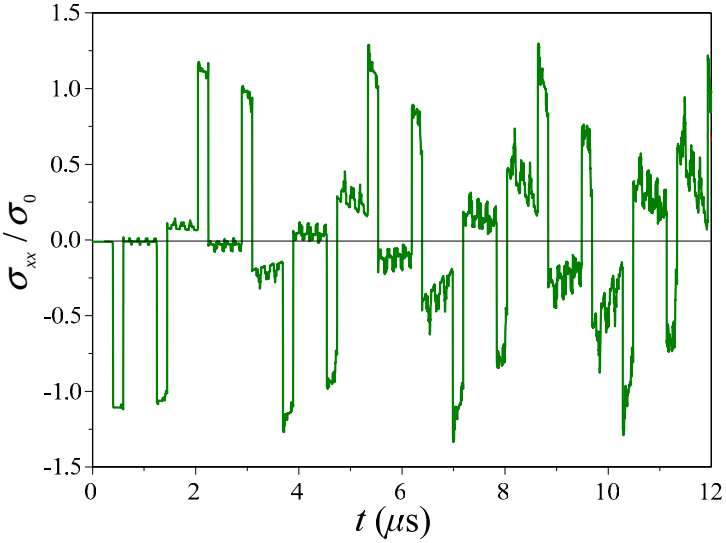

Figure 12: The stress response in a 10-layered medium (Ni/ZrO_2) at $x = l/2$ for fixed boundary condition at $x = 0$.

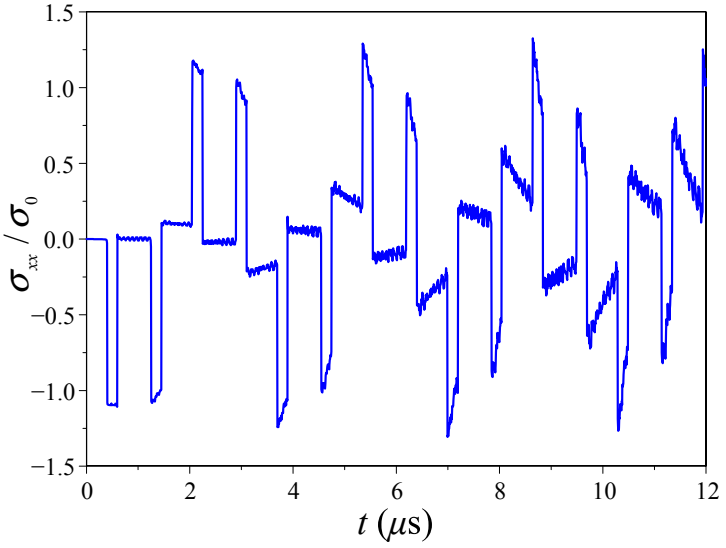

Figure 13: The stress response in a 20-layered medium (Ni/ZrO_2) at $x = l/2$ for fixed boundary condition at $x = 0$.

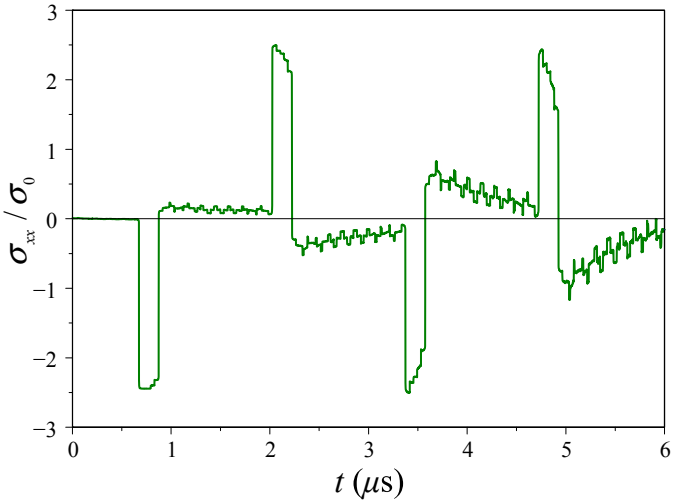

Figure 14: The stress response in a 10-layered medium (SiC/Al) at $x = 0$ for fixed boundary condition at $x = 0$.

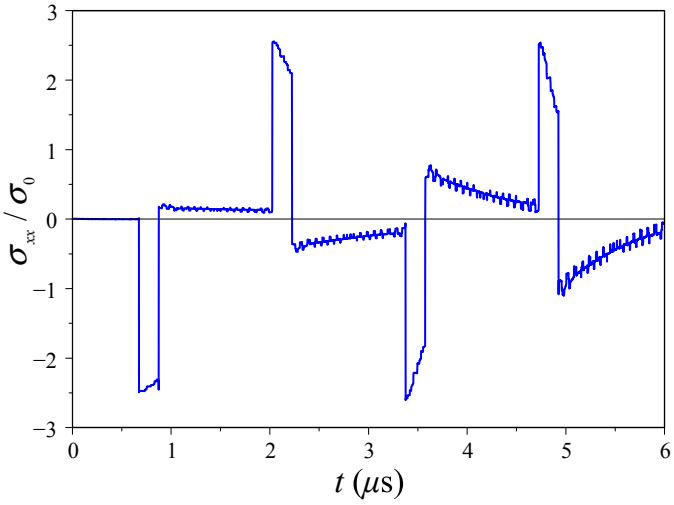

Figure 15: The stress response in a 20-layered medium (SiC/Al) at $x = 0$ for fixed boundary condition at $x = 0$.

Fig. 12 and Fig. 13. In Fig. 12, transient response of Ni/ZrO_2 FGM simulated by 10-layered medium is calculated up to $12\mu s$ at location $x = l/2$ for the boundary condition indicated in Fig. 1(b). If we use the 20-layered medium (related material constants are listed in Table 3) to simulate Ni/ZrO_2 FGM, the numerical result expressed in Fig. 13 is much closer to the FGM formulation. For the case of SiC/Al FGM, numerical results obtained by 10-layered and 20-layered media are shown in Fig. 14 and Fig. 15. In Fig. 14, transient response of SiC/Al FGM simulated by 10-layered medium is calculated up to $6\mu s$ at location $x = 0$ for the boundary condition indicated in Fig. 1(b). The same SiC/Al FGM is further divided into 20 layers (related material constants are listed in Table 5) and the result is shown in Fig. 15. We note that the amplitude of oscillation becomes smaller in Fig. 13 (Fig. 15) than that in Fig. 12 (Fig. 14), and this phenomenon indicates that more layers will result less impedance-mismatch and more closer to the result of FGM.

6 Conclusions

In this article, the transient response in FGM slab is analyzed by Laplace transform technique. The analytical solution is determined in the transform domain from the boundary conditions. A numerical Laplace inversion method (Durbin's formula) instead of Abel-Tauber asymptotic theorem (Chiu & Erdogan (1999)) is used to obtain the transient response in the time domain. From the consideration of accuracy and numerical efficiency, Durbin's formula is easy and capable to be used to investigate the wave-propagation problem of FGM for long-time calculation. In this study, we also use 10-layered and 20-layered homogeneous media to simulate the FGM slab. These two approaches have similar results. Oscillation phenomenon is found in multi-layered solutions which is due to the impedance-mismatch of the layer. When the number of layer increase, the magnitude of the oscillation decrease. It is concluded that the multi-layered formulation is capable to simulate the non-homogeneous FGM if the number of the layer is large enough. This multilayered formulation not only can be used for simulating the FGM with polynomial-form but also is applicable for the power-law or exponential-form of FGM.

Acknowledgement: The authors gratefully acknowledge Grant NSC 98-2923-E-002-003-MY3 from the National Science Council, Republic of China, to National Taiwan University.

References

Abu-Alshaikh, I.; Köklüce, B. (2006): One-dimensional transient dynamic response in functionally graded layered media. *J. Eng. Math.*, vol. 54, pp. 17-30.

Black, M.C.; Carpenter, E.W.; Spencer, A.J.M. (1960): On the solution of one dimensional elastic wave propagation problems in stratified media by the method of characteristics. *Geophysical Prospecting,* VIII, pp. 218-230.

Cai, H.; Bao, G. (1998): Crack bridging in functionally graded coatings. *Int. J. Solids Struct.*, vol. 35, pp. 701-717.

Chen, X.; Chandra, N.; Rajendran, A.M. (2004): Analytical solution to the plate impact problem of layered heterogeneous material systems. *Int. J. Solids Struct.*, vol. 41, pp. 4635-4659.

Chi, S.H.; Chung, Y. L. (2006): Mechanical behavior of functionally graded material plates under transverse load-part i: analysis. *Int. J. Solids Struct.*, vol. 43, pp. 3657-3674.

Chiu, T.C.; Erdogan, F. (1999): One-dimensional wave propagation in a functionally graded elastic medium. *J. Sound Vibr.*, vol. 222, pp. 453-487.

Delale, F.; Erdogan, F. (1983): The crack problem for a nonhomogeneous plane. *ASME J. Appl. Mech.*, vol. 50, pp. 609-614.

Durbin, F. (1974): Numerical inversion of Laplace transforms: an efficient improvement to Dubner and Abate's method. *Computer J.*, vol. 17, pp. 371-376.

Erdogan, F.; Wu, B.H. (1995): Crack problems in FGM layers under thermal stresses. *J. Therm. Stresses*, vol.19, pp. 237-265.

Han, X.; Liu, G.R. (2002): Effects of SH waves in functionally graded plate. *Mech. Res. Comm.*, vol. 29, pp. 327-338.

Han, X.; Liu, G.R.; Lam, K.Y. (2000): A quadratic layer element for analyzing stress waves in functionally gradient materials and its application in material characterization. *J. Sound Vibr.*, vol. 236, pp. 307-321.

Hegemier, G.A.; Nayfeh, A.H. (1973): A continuum theory for wave propagation in laminated composites. Case 1: propagation normal to the laminates. *ASME J. Appl. Mech.*, vol. 40, pp. 503-510.

Jabbari, M.; Sohrabpour, S.; Eslami, M.R. (2002): Mechanical and thermal stresses in a functionally graded hollow cylinder due to radially symmetric loads. *Int. J. Pres. Ves. Pip.*, vol. 79, pp. 493-497.

Jin, Z.H.; Paulino, G. H. (2001): Transient thermal stress analysis of an edge crack in a functionally graded material. *Int. J. Fracture*, vol. 107, pp. 73-98.

Jin, Z.H.; Batra, R.C. (1996): Stresses intensity relaxation at the tip of an edge crack in a functionally graded material subjected to a thermal shock. *J. Therm. Stresses*, vol.19, pp. 317-339.

Lee, J.M.; Ma, C.C. (2010): Analytical solutions for an antiplane problem of two

dissimilar functionally graded magnetoelectroelastic half-planes. *Acta Mechanica*, vol. 212, pp. 21-38.

Liu, G.R.; Han, X.; Lam, K.Y. (1999): Stress waves in functionally gradient materials and its use for material characterization. *Compos. B: Eng.*, vol. 30, pp. 383-394.

Lundergan, C.D.; Drumheller, D.S. (1971): Propagation of stress waves in a laminated plate composite. *J. Appl. Phys.*, vol. 42, pp. 669-675.

Ma, C.C.; Lee, J.M. (2009a): Theoretical analysis of in-plane problem in functionally graded nonhomogeneous magnetoelectroelastic bimaterials. *Int. J. Solids Struct.*, vol. 46, pp. 4208-4220.

Ma, C.C.; Lee, J.M. (2009b): Full-field analysis of a functionally graded magnetoelectroelastic nonhomogeneous layered half-plane. *CMES-Comp. Model. Eng.*, vol.54, pp. 87-120.

Mukunoki, I.; Ting, T.C.T. (1980): Transient wave propagation normal to the layering of a finite layered medium. *Int. J. Solids Struct.*, vol.16, pp. 239-251.

Narayanan, G.V.; Beskos, D.E. (1982): Numerical operational methods for time-dependent linear problems. *Int. J. Numer. Meth. Eng.*, vol.18, pp. 1829-1854.

Papoulis, A. (1957): A new method of inversion of the Laplace transform. *Quart. Appl. Math.*, vol.14, pp. 405-414.

Santare, M.H.; Thamburaj, P.; Gazoans, G.A. (2003): The use of graded finite elements in the study of elastic wave propagation in continuously non-homogeneous materials. *Int. J. Solids Structs.*, vol. 40, pp. 5621-5634.

Stern, M.; Bedford, A.; Yew, C.H. (1971): Wave propagation in viscoelastic laminates. *ASME J. Appl. Mech.*, vol. 38, pp. 448-454.

Sun, C.T.; Achenbach, J.D.; Herrmann, G. (1968): Time-harmonic waves in a stratified medium propagating in the direction of the layering. *ASME J. Appl. Mech.*, vol. 35, pp. 408-411.

Sun, C.T.; Achenbach, J.D.; Herrmann, G. (1968): Continuum theory for a laminated medium. *ASME J. Appl. Mech.*, vol. 35, pp. 467-475.

Tang, Z.; Ting, T.C.T. (1985): Transient waves in a layered anisotropic elastic medium. *Proc. R. Soc. Lond.*, vol. A397, pp. 67-85.

Ting, T.C.T.; Mukunoki, I. (1979): A theory of viscoelastic analogy for wave propagation normal to the layering of a layered medium. *ASME J. Appl. Mech.*, vol. 46, pp. 329-336.